

# Optical links for cryogenic focal-plane array readout

Alan R. Johnston, Duncan T.H. Liu, Siamak Forouhar,  
George F. Lutes, Joseph Maserjian, and Eric R. Fossum

Jet Propulsion Laboratory, California Institute of Technology  
Pasadena, CA 91109 USA

## ABSTRACT

An optical link can provide an interface channel for the focal-plane array that is immune to electromagnetic interference (EMI) and can lower the heat load on the dewar. Our approach involves the use of fiber-optics and an on-focal-plane optical modulator to provide an interface to the focal-plane array (FPA). The FPA drives the modulator with an electrical signal. We evaluated specially fabricated AlGaAs/GaAs multiple quantum well (MQW) optical modulators, operating near 840 nm, for analog modulation, and we have used the results to calculate the performance of an optical interface link using experimentally determined device parameters. Link noise and dynamic range for an analog link were estimated from a separate experiment using pigtailed fiber components. The performance of the MQW modulator system is compared to alternative strategies. Significant improvement in performance in comparison to conventional electronic interfaces appears to be possible.

## 1. Introduction

Optical instruments employing cryogenic focal-plane arrays must minimize power dissipation on the focal-plane. Since cooler power efficiency is low at cryogenic temperatures, reduction of focal-plane power has strong leverage in reducing total system power and cooler mass. Technologies that can reduce total focal-plane power dissipation, increase focal-plane capability, reduce system power needs, or minimize instrument size and mass are of great interest for maximizing mission lifetime. The cabling between the dewar and the external warm electronics is susceptible to EMI and thus reduced signal-to-noise (SNR) performance and also provides additional leakage paths for heat to enter the cryogenic system. Reduction in cable channel count can also lead to an increase in system reliability.

Optical interconnects are currently a topic of interest for many electronic and opto-electronic systems.<sup>1</sup> The interconnects can be either free-space or guided. The study of guided interconnects (e.g. optical fibers) is driven by the advantages they offer in freedom from EMI and potential bandwidth. Free-space interconnects, while requiring a high degree of mechanical stability and line-of-sight clearances between optical components, offer the possibility of high density interconnects, since optical beams can cross in free space without interaction. The potential for optical interconnects in cryogenic dewar systems has been recognized for several years, but only recently has activity in this area been reported<sup>2,3</sup>.

In comparison to optical communications applications, where optical data communication speeds exceed 1 Gbit/sec, the focal-plane application of optical interconnects requires relatively low frequency operation, e.g. from 50 kHz for scientific applications to 100 MHz for some infrared seekers. For the transmission of scientific pixel data, approximately 12-14 bits of dynamic range are required. For FLIR and other non-scientific applications, there is a trade-off made for less dynamic range but higher data rate. In a typical scientific system, the electronic multiplexer's output amplifier dissipates approximately 10 mW of power on the focal-plane. In higher data rate systems, this can rise to 100 mW dissipated on the focal-plane.

In this paper, we explore the use of a fiber optic link between the cryogenic focal-plane and the external electronics to replace conventional metallic cabling and electrical interfaces. Our general approach is to locate an optical source, such as a semiconductor laser, outside the dewar in a warm environment where power dissipation is less critical. The light is transmitted to the focal-plane where it is modulated, and the optical signal is then transmitted to the warm environment where it can be detected and analyzed. Both digital and analog signals are under consideration. The optical link approach is explored both analytically and experimentally. In particular, an analysis of the system SNR is performed for the optical

link in terms of total focal-plane power dissipation. Dynamic range is also defined and analyzed. The nonlinearity of the optical link is also discussed. Options and trade-offs such as power dissipation versus speed are considered. Experimental measurements made with an AlGaAs/GaAs MQW modulator are reported, and the noise-limited dynamic range of a test link was measured.

## 2. Optical Link Configuration

The optical readout link configuration we are considering is illustrated in Figure 1. The figure shows a focal-plane array (FPA) and a separate optical waveguide modulator chip mounted in close proximity to it on a common substrate, providing for a minimum length electrical interconnect between the two. The entire assembly is mounted within a dewar at the instrument focal-plane. The use of a fiber rather than free-space optics, and a single, rather than multichannel, configuration is essentially an assumption at this point. Alignment of the fiber to the modulator is a critical step, but it can be done under controlled conditions during fabrication. The parts can be cemented into an integral assembly, which maintains alignment thereafter. In addition, the use of fiber optics allows for the readout light to be readily isolated from the FPA by opaque coatings. The focal-plane array itself is assumed to contain circuitry for multiplexing the detector signals into a single serial output, and to provide suitable gain to match the output signal levels to the requirements of the modulator. The required signal level can be set between 0.25 and 4 V, by design.

The modulator, seen in Figure 2, is an AlGaAs/GaAs MQW waveguide device fabricated on a chip 100 to 200  $\mu\text{m}$  long and perhaps 100  $\mu\text{m}$  wide. The use of a modulator of this type for modulation by a low-voltage signal was described by Wiener et al <sup>4</sup>. Its structure is very similar to that of a laser, with the active waveguide region being a few microns deep and less than 10  $\mu\text{m}$  wide. Fiber pigtailed are used as the mechanism for coupling light into and out of the modulator chip, using the same techniques commonly used to make a fiber-pigtailed laser. Note that an alternative configuration could be set up with the modulator working in reflection, using the same fiber for both input and output. In this case, a fused coupler outside the dewar would separate the incoming laser beam from the modulated output signal. However, a fundamental problem from increased link noise would have to be dealt with. This possibility is available for future consideration, but will not be discussed here.

A single mode polarization-preserving fiber must be used between the laser and the modulator because the MQW device is polarization sensitive. A large core, multimode fiber will suffice between the modulator and the receiver outside the dewar. The use of such a fiber would ease the alignment requirements at the output facet of the modulator. The laser and the fiber link design must both be optimized for low noise. The laser wavelength must be carefully matched to the absorption band of the cooled modulator, which will be significantly shifted in wavelength compared to its room temperature value. Actually, it will be desirable to tailor the modulator wavelength to match the laser in order to take advantage of existing off-the-shelf lasers developed for communication applications. The optical receiver can be a typical low-noise fiber-pigtailed detector-preamp module designed for analog communication applications but modified to optimize its noise over an appropriate band, for example 0-1 Mhz, for this application.

## 3. Analysis

### 3.1. Readout link noise and dynamic range

In this section we calculate the theoretical dynamic range of the readout link, and relate it to readout bandwidth, modulation index, and optical power.  $P_l$  is the coupled power from the laser,  $P_m$  is the power incident on the modulator,  $A$  is an attenuation introduced between laser and modulator, and  $P_r$  is the power delivered to the optical receiver.

These quantities can be followed through the system using the following expressions:

$$P_m = AP_l \tag{1}$$

$$P_r = \alpha P_m (1 - fM) \tag{2}$$

The representation of the modulator, equation (2), is arbitrarily set up such that the quantity  $\alpha$  is the total insertion loss of the modulator at maximum transmission. The modulation index,  $M = [P_r(max) - P_r(min)]/P_r(max)$ , and  $f(0 < f < 1)$  is a time-varying parameter representing the modulator input signal.  $P_r(max)$  occurs for  $f=0$  and  $P_r(min)$  for  $f=1$ . The quantity  $S = P_r(max) - P_r(min) = \alpha M P_m$  is the maximum signal swing, also measured at the receiver input.

The laser noise, usually called relative intensity noise (RIN) is given by  $\delta P_i^2 = P_i^2 B \cdot RIN$ <sup>5</sup>. The quantum noise,  $\delta P_q$ , is given by

$$\delta P_q = \left( \frac{2h\nu B P_r}{\eta} \right)^{1/2} \quad (3)$$

where  $h\nu$  is the quantum energy, ( $2 \times 10^{-19}$  at  $\lambda = 1 \mu m$  in mks units) and  $\eta$  is the quantum efficiency of the detector.  $B$  is the signal bandwidth, which is defined in our system by the receiver module.

The quantities  $\delta P_r$ ,  $\delta P_q$ , and  $\delta P_i$  represent the RMS value of receiver noise, quantum noise, and laser noise, respectively, all measured in terms of an equivalent optical noise power at the receiver input. The three principal system noise terms, normalized by the signal swing  $S$ , are:

$$\text{Relative detector noise} \quad \left( \frac{\delta P_r}{S} \right) = \frac{\sqrt{B}}{M} \frac{NEP}{\alpha P_m} \quad (4)$$

$$\text{Relative quantum noise} \quad \left( \frac{\delta P_q}{S} \right) = \frac{\sqrt{(1-M)B}}{M} \sqrt{\frac{2h\nu}{\eta \alpha P_m}} \quad (5)$$

$$\text{Relative laser noise} \quad \left( \frac{\delta P_i}{S} \right) = \left( \frac{1-M}{M} \right) \sqrt{B} \sqrt{RIN} \quad (6)$$

The magnitude of each of these terms can be understood as a reciprocal of dynamic range, and they combine in RSS fashion to give the total system noise. They are plotted in Figure 3, for the parameter values given in Table 1, as a function of  $P_m$ . It should be kept in mind that the quantum noise given by eq (5) represents an optimum theoretical performance. A real optical receiver, especially if required to provide a high dynamic range, will have a somewhat poorer performance. Current in biasing resistors required for the detector to operate properly over the entire dynamic range will add to the noise<sup>6</sup>. A  $RIN$  of -165 db/Hz, which can be reached with the quietest lasers, will produce a negligible contribution to the total system noise. On the other hand, off-the-shelf multimode diode lasers are much noisier. A  $RIN = -125$  db/Hz is typical, and would sharply limit link dynamic range.

Table I – Parameter Values Used in Figure 3

Insertion Loss of Modulator	$\alpha$	0.2
Signal Bandwidth	$B$	1.0 MHz
Modulation Index	$M$	0.5
Receiver equivalent input noise	NEP	-95.0 dbm/Hz <sup>1/2</sup>

The total relative noise can be scaled to a different system bandwidth by moving all curves vertically by a factor  $\sqrt{B/B_o}$ ,  $B_o$  being the assumed 1 Mhz bandwidth. In the region of operation important for a high dynamic range analog link, the quantum noise term (eq. 5) will dominate. The factor  $(1-M)^{1/2}/M$  describes its dependence on modulation index. Roughly a factor of 4 improvement in relative noise could be obtained by increasing  $M$  from 0.5 to 0.9, at the cost of a much larger nonlinearity.

### 3.2. Electrical drive power for the modulator and nonlinearity

The preceding analysis did not depend on the details of the modulator; only on the range of its optical transmission. However, nonlinearity and the drive voltage requirement, and with it the electrical drive power, do depend on the transfer function of the modulator. The capacitance of the modulator will be dominated by the interconnection between the FPA and the modulator chip. The electrical power  $P_e$  required to drive the modulator is  $P_e = 2(1/2 CV^2 f)$ . For  $f = 1$  MHz, FPA output signal  $V = 1$  V, and  $C = 1$  pf,  $P_e$  becomes  $\sim 1$   $\mu$ W, negligible in comparison to the typical values of  $P_m$  which would be needed to achieve a dynamic range of several thousand.

A crude estimate of nonlinearity can be made by approximating the modulator voltage transfer function by a raised cosine function. For  $M = 0.5$ , the estimated departure from linearity is  $\pm 1/2\%$  from the best fit straight line. The nonlinear term, again very crudely, will vary as  $M^3$ .

## 4. Experimental Results

### 4.1. MQW device characterization

Figure 4 shows the layer structure of the MQW waveguide modulator which was grown in the JPL Microdevices Laboratory by MBE in a Riber 3200 system. Ohmic contacts were evaporated on the device, and it was then mounted on a laser mount and wire bonded.  $I-V$  curves were measured with and without incident light, respectively. To induce 1  $\mu$ A of photocurrent, the output power must be increased to about 360  $\mu$ W. Therefore, the power dissipation due to photocurrent will be negligible. In all the absorption and transmission measurements, the output power from the waveguide is less than 1  $\mu$ W.

A Spectra-Physics Model 3900 Ti:Sapphire laser was used to characterize the modulator. Figure 5 shows the relative absorption spectra of the MQW waveguide modulator for different voltages. It shows that the exciton energy without applied voltage is 1.49 eV which corresponds to  $\lambda = 830$  nm. As expected, the exciton energy is shifted to a lower value when the waveguide is reverse biased and to a higher value when the waveguide is forward biased. Furthermore, the exciton peak is broadened as the MQW waveguide is reverse biased. We estimated that the maximum modulation should occur near the tail of the exciton absorption curve at zero applied voltage or about 843 nm. Operating at this wavelength, the signal that drives the modulator will reverse bias the modulator. Because the absorption decreases as the voltage increases, the modulated light is full-on when there is no signal.

Figure 6 shows the voltage transfer functions for different wavelengths. In the reverse-biased region, the applied voltage can be as large as 10 volts without causing breakdown. In the forward-biased region, the waveguide starts to emit light at 0.85 volts. As expected, the largest modulation takes place at  $\lambda = 843$  nm. More data points for this wavelength were taken and plotted in Figure 7(a). To check the linearity of the 50% modulation region shown in the box in Figure 7(a), it is blown up and plotted in Figure 7(b). The solid line in Figure 7(b) is the linear least square fit of the experimental data. The nonlinearity is estimated to be less than 1% within the 50% modulation limit.

### 4.2. Link noise measurement

An experimental determination of the noise-limited dynamic range of an externally modulated fiber link was made to compare with our theoretical estimate. The fiber optic link was made up of an Ortel 3612B-E01 transmitter, a Crystal Technology MZ 313P lithium niobate waveguide modulator, and an optical receiver assembled in our lab. The noise signal out of the receiver amplifier was applied to a spectrum analyzer and the noise floor was measured over two ranges, 1 kHz to 100 kHz and 1 to 40 MHz. The reading was normalized to 1 Hz bandwidth. The waveguide modulator was replaced with an attenuator for these measurements to avoid the effort necessary to reduce noise peaks from back reflections. The modulator was used to measure the signal swing.

The results of the noise floor measurement for the frequency range from 1 kHz to 100 kHz are shown in Fig. 8. The noise floor curve for the 1 to 40 MHz range was virtually flat, at the  $-167$  dbm/Hz level over the entire frequency range.

For both frequency bands, the noise floor signal level is given in terms of an RF power at the output of the optical receiver. It is proportional to the square of the equivalent optical input power to the detector. Note that there is a slight slope to the measured noise vs frequency in the 1 to 100 kHz range, which is consistent with the difference in measured noise levels between the 100 kHz and the 1 MHz points. The peak near zero frequency is a combination of  $1/f$  noise and pickup, from 60 Hz and its harmonics. The peaks at 26 kHz and 52 kHz are also pickup from local noise sources. These noise peaks are typical in measurements of this type, and are very difficult to eliminate. The  $-167$  dbm/Hz figure is the RIN of the laser transmitter, since the carrier intensity was 1 mW. The measured dynamic range (signal swing  $\div$  noise) was 126 db/Hz at 100 kHz and 137 db/Hz at 1 MHz. Correcting it to be consistent with  $B = 1$  MHz and  $M = 0.5$ , one obtains the data point shown in Figure 3, which falls above the calculated line by a factor of 3. The agreement seems satisfactory.

## 5. Discussions and Conclusions

Our results indicate that readout of a focal plane array using fiber optics is feasible, and can achieve a significant reduction in the heat load on the focal plane. In addition, cross talk in the readout link itself will be reduced, and heat conduction by the readout cabling will also be decreased. The calculated link performance indicates that for a representative focal-plane-array requirement (1 – 2 Mhz signal bandwidth), the heat load in the dewar resulting from the readout link could be a few tenths of a milliwatt, assuming a dynamic range of 5000. This compares to approximately 60 mw dissipation measured for a conventional electronic output amplifier providing similar performance. The bandwidth of the readout link is not limited by any characteristic of the link; analog fiber-optic data transmission is being actively pushed into the microwave region<sup>7 8 9</sup>. However, the inherent power speed tradeoff would require increased power dissipation on the focal plane at a higher data rate. For example, in order to provide a 100 Mhz signal bandwidth, the link dissipation would become several tens of mW to maintain the assumed dynamic range of 5000. This cryogenic heat load is dominated by the optical power input to the modulator because most of it is dissipated in the modulating element. The electrical power required to drive the modulator is negligible. Thus the most effective step toward improving the link power dissipation would be to lower the insertion loss of the modulator. The best achievable value of insertion loss is probably near 3–4 db, limited by the coupling from the cylindrical fiber core to the planar modulator waveguide. We have assumed 7 db in our analysis.

Dynamic range in the operating regime of interest is limited by quantum noise (equivalent to shot noise in the photocurrent) in the optical signal. Detector noise, for a well designed receiver module, will be swamped out by the relatively high optical signal level. In general, dynamic range can be increased by increasing the power incident on the modulator, so an inherent tradeoff results between dynamic range and heat load. The effect of laser noise (RIN noise) for a diode laser source can be made negligible if optimum techniques are used. However, note that it is extremely important to minimize or eliminate all back reflections that could return part of the optical signal to the laser. Diode lasers are very sensitive to back reflection and their RIN can easily be increased by 40 db (2 orders of magnitude in terms of optical noise power) if back reflections are significant. In such a case, the system dynamic range will be limited by laser noise, and further improvement of dynamic range by increasing the link power is no longer possible. Angle polished connectors, non-reflecting attenuators, optical isolators, and optimum antireflection treatment of the modulator to fiber coupling should all be incorporated<sup>10</sup>.

There are alternative configurations for an optical readout link that we have considered briefly in this work. The alternatives involve three areas: first the type of optical modulator, second, the use of parallelism in the readout, which is often cited as an inherent strong point for optics, and third the possibility of digital readout.

Waveguide modulators of the Mach-Zender or delta-beta types could be used in place of the MQW modulator we investigated. An advantage of this type of modulator is a potential decrease in optical insertion loss. They are phase modulators with no absorption being involved in the modulation process. MQW modulators can be configured to work in a phase mode, and there are indications that a very strong phase effect can be realized in MQW structures<sup>11</sup>. Alternatively, phase modulators using either  $\text{LiNbO}_3$ <sup>12 13 14</sup>, or non-linear polymers<sup>15 16</sup> could be used. There are no known materials limitations that would preclude using either of these at cryogenic temperatures. As a practical matter, the difficulty of coupling a fiber to a planar waveguide is a similar limitation in all these modulator types. Further, the modulating voltage requirement of either  $\text{LiNbO}_3$  or NL polymer modulators appears to be somewhat larger, and their physical size is very much larger than the MQW type. On balance, it seems that the MQW modulator is the best choice.

A brief look at the possible advantages of a highly parallel (and therefore lower bandwidth) readout structure is inconclusive at this point. For example, a scaling analysis showed that multiple fiber links, one for each row (or pixel) do not use significantly less power in total. Free space optics could be used to eliminate the need for a large number of fibers in a highly parallel readout arrangement. However, the use of free-space optics would greatly complicate the design of the focal plane configuration, in order to rigorously separate the readout light from the low-level image light, and also to maintain alignment between the optical components inside and those outside of the dewar.

The scaling analysis did indicate that a different type of parallelism, namely one where the dynamic range of the output signal is subdivided (of which digital encoding is one example) can result in a significant power saving. For a digital readout link, the conclusion seems quite clear cut; it performs much better than an equivalent analog one. A digital link is essentially an ideal channel, both in terms of fidelity and power, in comparison to other elements of the system. However, the challenge has simply been transferred to an A/D circuit which must now be incorporated in the focal plane. It is not yet clear whether an overall net improvement in performance can be achieved, but related topics are being actively pursued<sup>17 18 19</sup>.

Several things remain to be done before successful hardware can be implemented. The most important issue is to determine what effects the cryogenic environment will have on the parts of the readout link that will be located in the dewar. Changes in modulator parameters can be expected, as well as mechanical effects from differential expansivity. The working optical wavelength of the modulator will decrease, and its transfer function should become steeper. There is no performance penalty expected from the wavelength shift, but it is a large shift, expected to be about 50 nm, and must be allowed for in design. The change to be expected in the slope of the modulation curve is not known at this point, but it should be small. Equally important, the effect of thermal strains associated with the mounting of the modulator chip and the fiber pigtailed can be critical. Development of practical fabrication techniques that will withstand the thermal cycling without causing an unacceptable impact on performance is vital. The insertion loss at maximum transmission is a very important parameter. Optimization of the fiber to modulator chip coupling is needed, and is closely related to the mechanical thermal design issue. Finally, in order for an optical readout link to function properly in a system sense, suitable electronic stabilization techniques must be developed to maintain the desired operating conditions and with them the calibration of the readout process.

## 6. Acknowledgements

We would particularly like to thank Anders Larsson, now at Chalmers University, Goteborg, Sweden, who was involved in early discussions about the idea, before the present task began. The MBE work to produce the wafers from which our test devices were made was carried out by John Liu and Robert Conley in JPL's Microdevices Laboratory. The test devices were prepared by Sam Keo, also in the Microdevices Laboratory. Finally, we thank Thomas Wood of ATT Bell Laboratories for helpful discussions about the modulating devices, and Frank Jaworski of Loral, Inc., Lexington, MA, who provided insights into present-day system applications.

The work described in this paper was supported by the JPL Director's Discretionary Fund. It was carried out as part of the Center for Space Microelectronics Technology Program at the Jet Propulsion Laboratory, California Institute of Technology, and was sponsored by the National Aeronautics and Space Administration. Reference herein to any specific commercial product, process, or service does not imply its endorsement by the United States Government, NASA, or the Jet Propulsion Laboratory, California Institute of Technology.

## 7. References

1. See for example Batchman et al, "Optoelectronic Materials, Devices Packaging and Interconnects," SPIE Proceedings, Vol. 836 (1987); McWright et al, "Optoelectronic Materials, Devices, Packaging and Interconnects II," SPIE Proceedings, Vol. 994, 1988.
2. Eric R. Fossum, "Photonic Interconnections: More Bandwidth, Less Real Estate," *Photonics Spectra*, May 1987.
3. Eric Fossum, A.G. Larsson, Joseph Maserjean, "Optical Link for Readout from a Focal Plane Array," *NASA Tech Brief*, Vol 16, No. 10, page 30–31, Oct. 1992.

4. J.S. Weiner, A.C. Gossard, J.H. English, D.A.B. Miller, D.C. Chemla, and C.A. Burrus, "Low-Voltage Modulator and Self-Biased Self Electro-Optic Device," *Electr Lett* **23**, 75, 1987.
5. G.P. Agrawal and N.K. Dutta, *Long-wavelength Semiconductor Lasers*, page 247, Van Nostrand Reinhold, 1986.
6. T.V. Muoi, "receiver Design for High Speed Fiber Optic Systems," *J Lightwave Tech.*, **LT-2**, 243, 1984.
7. W.E. Stephens and T.R. Joseph, "System characteristics of direct modulated and externally modulated RF fiber-optic links," *J. Lightwave Technology*, **LT-5**, 380, 1987.
8. G.E. Betts, L.M. Johnson, and C.H. Cox, III, "High Dynamic range, low-noise analog optical links using external modulators: analysis and demonstration," *SPIE Proceedings*, Vol. 1562, 281, 1990.
9. G.E. Betts, L.M. Johnson, and C.H. Cox III, "Optimization of externally modulated analog optical links," *SPIE Proceedings*, Vol. 1562, 281, 1991.
10. R.T. Logan and G.F. Lutes, "High Stability Microwave Fiber Optic Systems: Demonstrations and Applications," *Proceedings, 46th Annual Symposium on Frequency Control*, Hershey, PA, May 27–29, 1992; R.T. Logan, G.F. Lutes, L.E. Primas, L. Maleki, "Design of a Fiber Optic Transmitter for Microwave Analog Transmission with High Phase Stability," *Proceedings, AFCEA Fiber Optics Conference '90*, McLean, VA, March 20–23, 1990.
11. C. Thirstrup, "Novel electro-optical phase modulator based on GaInAs/InP modulation doped quantum-well structures," *Appl. Phys. Lett.*, **61**, 2641 (1992).
12. H. Kogelnik & R.V. Schmitt, "Switched directional couplers with alternating  $\Delta\beta$ ," *IEEE JOE* **QE-12**, 396, 1976.
13. R.C. Alferness, "Waveguide Electrooptic Modulator," *IEEE Trans Microwave Theory & Tech*, **MTT-30**, 1121, 1982.
14. See for example waveguide modulator, Model 4531, (made by United Technologies Photonics) New Focus, Mountain View CA,
15. Van Tomme, *IEEE JOE* **27**, 778, 1991.
16. Van Tomme, *J. Appl Phys.* **69**, 6273, 1991.
17. Tushar R. Gheewala, "Josephson-Logic Devices and Circuits," *IEEE Trans Electron Devices*, **ED-27**, 1857, 1980.
18. K.K. Likharev and V.K. Semenov, "RFSQ Logic/Memory Family: A new Josephson Junction Technology for Sub Terahertz Clock Frequency Digital Systems," *IEEE Trans. Appl. Superconductivity*, **1**, 3, 1991.
19. E.A. Vittoz, "The Design of High-Performance Analog Circuits on Digital CMOS Chips," *IEEE J. Solid State Circuits*, **SC-20**, 657, 1985.

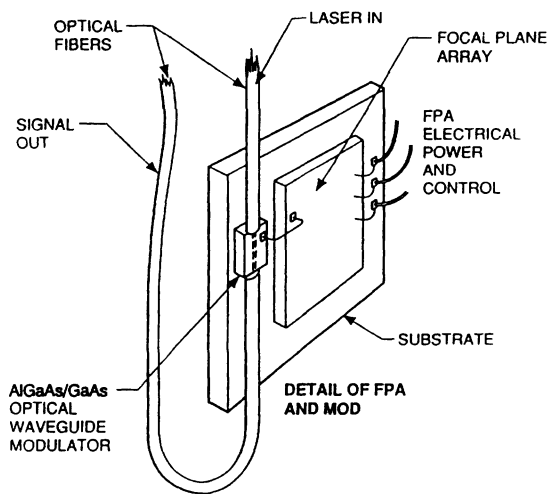


Figure 1. A sketch illustrating the readout link concept.

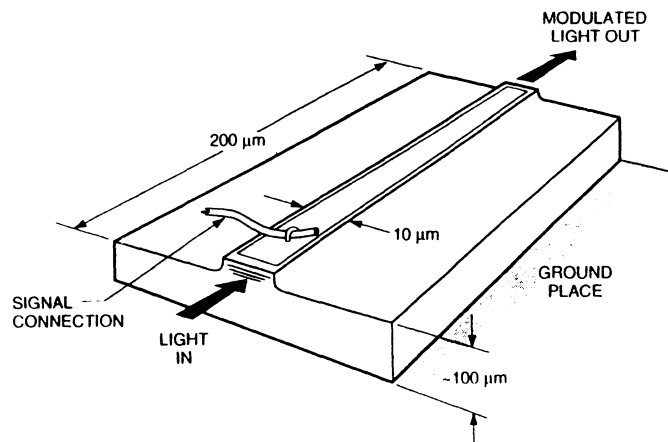


Figure 2. A sketch of the MQW modulator.

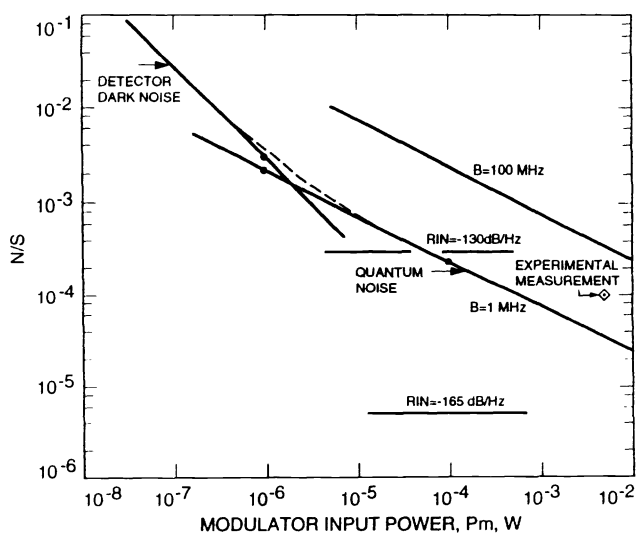


Figure 3. Link relative noise vs modulator input power.

Thickness	Material	Dopant Concentration
1000Å	GaAs:Be	1E19
9000Å	GaAs:Be	1.43E18
17600Å	Al.3Ga.7As:Si	1E18
870Å	Al.3Ga.7As	
90Å	GaAs	
80Å	Al.3Ga.7As	
90Å	GaAs	
387Å	Al.3Ga.7As	
18100Å	Al.3Ga.7As:Si	1E18
3000Å	GaAs:Si	1.43E18
GaAs Substrate		

1517Å Field Region

3.72 μm Waveguide Region

Figure 4. Layer structure of the test MQW waveguide modulator.

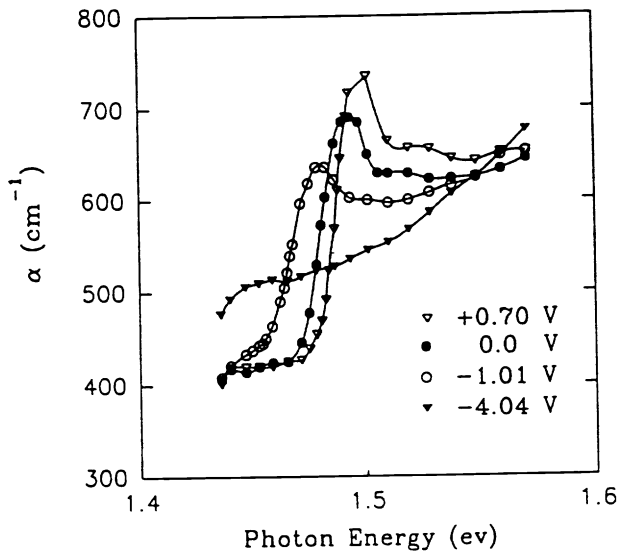


Figure 5. Absorption spectrum of the test MQW waveguide modulator at various applied voltages.

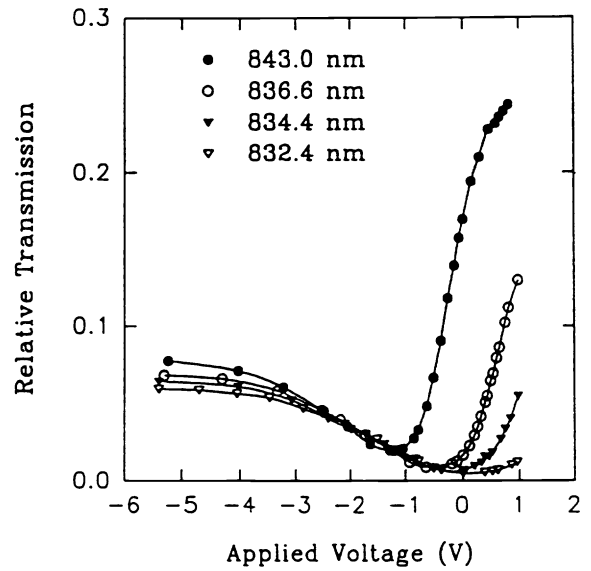


Figure 6. Relative transmission vs applied voltage of the test MQW modulator at various wavelengths.

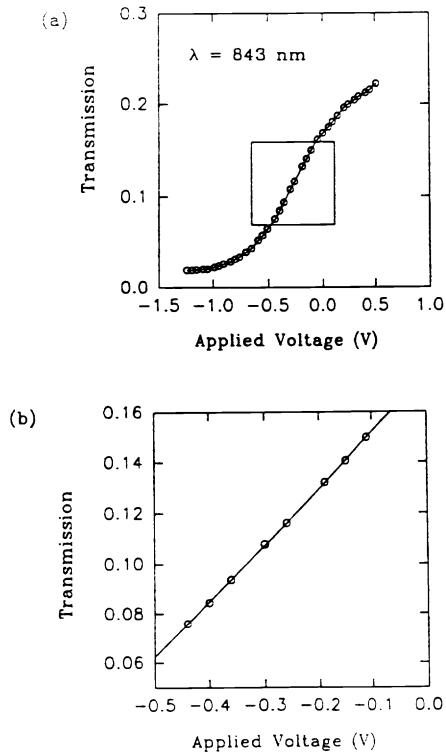


Figure 7. Modulation transfer function, optical transmission vs applied voltage at  $\lambda = 843$  nm. a) Complete curve; b) Magnified plot of the boxed region in a).

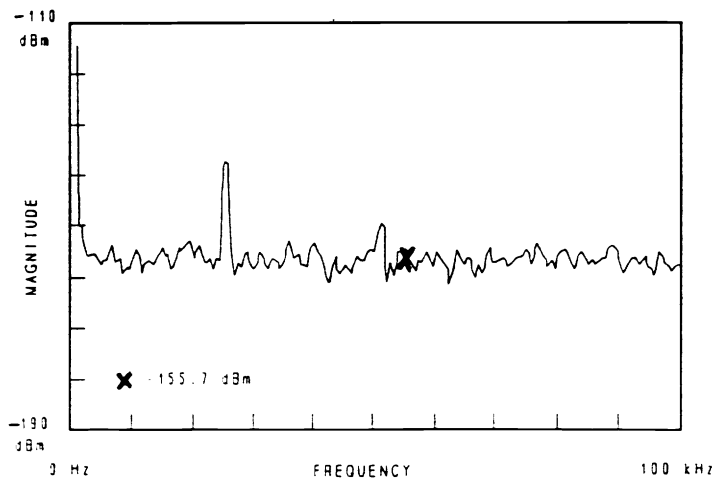


Figure 8. Measured noise vs frequency spectrum of link output from 0 to 100 kHz.